Received: 17 March 2017 | Revised: 16 May 2017 | Accepted: 24 June 2017

DOI: 10.1111/cbdd.13069

RESEARCH ARTICLE

WILEY

Novel pyrrolocycloalkylpyrazole analogues as CB_1 ligands

Battistina Asproni[1] | **Ilaria Manca**[2] | **Giansalvo Pinna**[1] | **Elena Cichero**[3] | **Paola Fossa**[3] | **Gabriele Murineddu**[1] | **Paolo Lazzari**[2] | **Giovanni Loriga**[4] | **Gérard A. Pinna**[1]

[1]Dipartimento di Chimica e Farmacia, Università degli Studi di Sassari, Sassari, Italy

[2]KemoTech Srl, Pula, CA, Italy

[3]Dipartimento di Farmacia, Università di Genova, Genova, Italy

[4]Consiglio Nazionale delle Ricerche, Istituto di Farmacologia Traslazionale, UOS Cagliari, Pula, CA, Italy

Correspondence
Battistina Asproni, Dipartimento di Chimica e Farmacia, Università degli Studi di Sassari, Sassari, Italy.
Email: asproni@uniss.it

Novel 1,4-dihydropyrazolo[3,4-*a*]pyrrolizine-, 4,5-dihydro-1*H*-pyrazolo[4,3-*g*]indolizine-and1,4,5,6-tetrahydropyrazolo[3,4-*c*]pyrrolo[1,2-*a*]azepine-3-carboxamide-based compounds were designed and synthesized for cannabinoid CB_1 and CB_2 receptor interactions. Any of the new synthesized compounds showed high affinity for CB_2 receptor with K_i values superior to 314 nM, whereas some of them showed moderate affinity for CB_1 receptor with K_i values inferior to 400 nM. 7-Chloro-1-(2,4-dichlorophenyl)-*N*-(homopiperidin-1-yl)-4,5-dihydro-1*H*-pyrazolo[4,3-*g*]indolizine-3-carboxamide (**2j**) exhibited good affinity for CB_1 receptor ($K_i CB_1 = 81$ nM) and the highest CB_2/CB_1 selectively ratio (>12). Docking studies carried out on such compounds were performed using the hCB_1 X-ray in complex with the close pyrazole analogue AM6538 and disclosed specific pattern of interactions related to the tricyclic pyrrolopyrazole scaffolds as CB_1 ligands.

KEYWORDS
binding affinity, cannabinoid receptors, docking studies, pyrrolocycloalkylpyrazole

1 | INTRODUCTION

The cannabinoid CB_1 and CB_2 receptors (CB_1R and CB_2R) belong to the rhodopsin-like family of G protein-coupled receptors (GPCRs) and are key components of the endocannabinoid system.[1–3] The CB_1R is abundantly expressed in the central nervous system (CNS) but also is present in peripheral tissues, including lungs, liver, kidneys and adipocytes.[4] CB_2R is found most abundantly in the periphery, predominantly expressed in cells of the human immune system as spleen, tonsils and thymus,[4] and to a much lesser extent in CNS.[5] CBRs are activated by terpenoid plant constituents, for example, by Δ^9-tetrahydrocannabinol, the major psychoactive component of *Cannabis sativa*.[6] Recent studies have demonstrated that CB_2Rs are involved in numerous diseases.[4,7] Several selective CB_2R agonists exhibited analgesic activity in preclinical models of acute, inflammatory and neuropathic pain,[4,8,9] whereas CB_1R activation mediates analgesia, stimulation of appetite and euphoria, among other effects,[4] and is responsible of psychotropic effects.[10] CB_1R antagonists are potential drugs for the therapy of drug and alcohol addiction as well as for the treatment of obesity. In this regard, rimonabant (Figure 1) was the first potent CB_1R antagonist/inverse agonist[11] approved by European Commission as an antiobesity agent; however, it was soon withdrawn by EMEA for its serious psychiatric disorders including anxiety, depression and suicidal tendency.[12] Within the search for new and safe antiobesity agents, recent medicinal chemistry approaches are oriented towards the obtainment of new peripherally selective CB_1 antagonists, by designing ligands that do not cross the blood–brain barrier and have low brain penetration.[13–15] The relevance of CBRs as emerging target of pharmacotherapy is documented also by the discovery of peripherally mixed CB_1R/CB_2R agonists as antiglaucoma agents.[16]

During the past decade, numerous ligands endowed with high affinity and subtype selectivity for both receptors were synthesized, and within each chemo-type the structure–activity relationship (SAR) studies were explored.

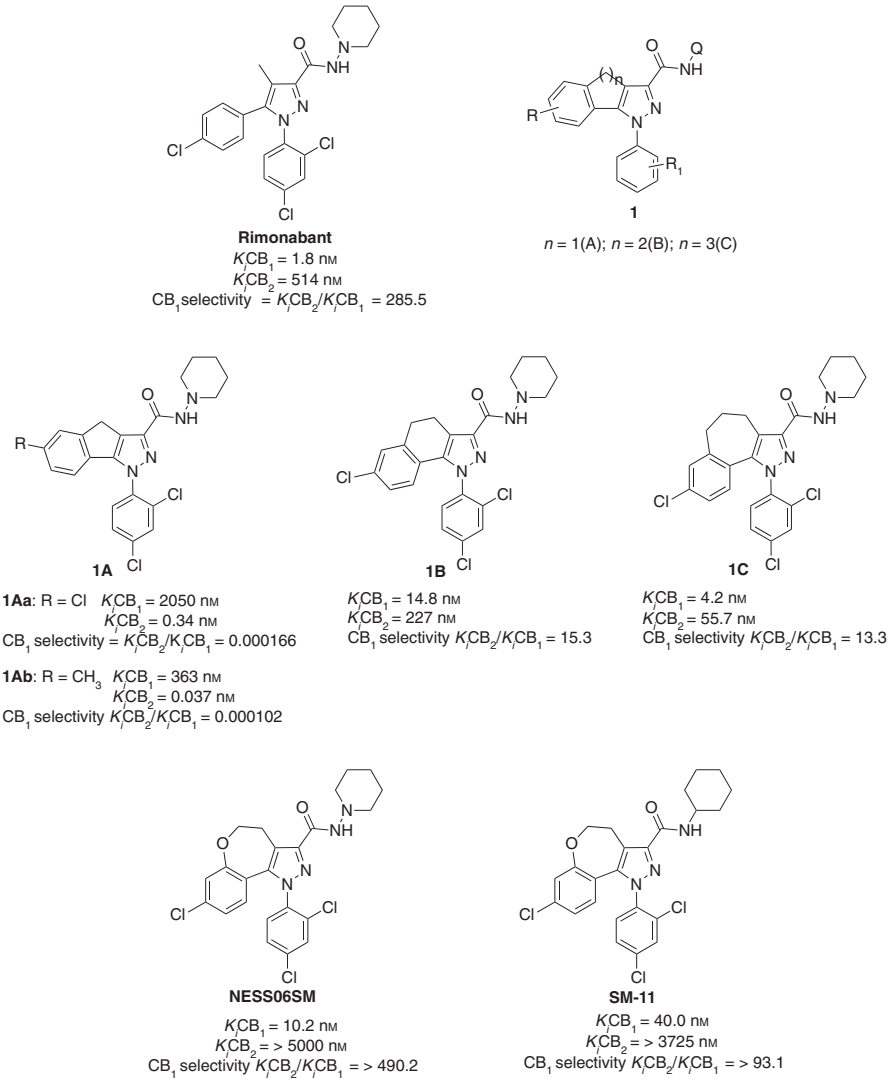

FIGURE 1 Chemical structures of CBRs ligands

The 4-alkyl-5-arylpyrazole skeleton of rimonabant has been modified by us (Figure 1), giving rise to 1,4-dihydroindeno[1,2-*c*]pyrazole **1A**,[17] 4,5-dihydro-1*H*-benzo[*g*]indazole **1B**[18] and 1,4,5,6-tetrahydrobenzo[6,7]cyclohepta[1,2-*c*]pyrazole-based ligands **1C**.[19] Such tricyclic systems feature a carbamoyl group at position 3 and simple substituents (halogen, methyl, methoxy) on the aryl moieties. These compounds displayed interesting cannabinoid binding affinity and subtype selectivity. In particular, changes in the size and shape of the tricyclic unit in ligands **1** revealed intriguing effects on the biological activity. Thus, increasing the length of the carbon bridge between C_4 of the pyrazole and the 4-chlorophenyl group from one to three methylene units led to a marked increase in the CB_1 binding affinity and selectivity. Moreover, the presence of a substituent, such as F, Cl, Br or CH_3, on the phenyl ring of the tricyclic system generally gave an increase in the affinity and selectivity for CB_2R. Compounds **1Aa**, **1Ab**, **1B** and **1C** are representatives of this class of CB ligands. The pharmacological relevance of these compounds emerged from the ability of the CB_2 agonist **1Ab** in alleviating neuropathic pain through functional microglia changes in mice.[20] Furthermore, the analogues CB_1 antagonist compounds NESS06SM and SM-11, featuring the 4,5-dihydrobenzo-oxa-cycloheptapyrazole skeleton could represent useful candidate agents for the treatment of obesity and its metabolic complications.[21]

Continuing with our interest in expanding SAR studies on CBRs,[22] we have undertaken a study to prepare new CB ligands related to both rimonabant and its derivatives **1**. Thus, driven by our understanding of the biological and pharmacological behaviour of the tricyclic pyrazoles, we explored a series of new tricyclic scaffolds incorporating the biologically interesting pyrrole and pyrazole moieties with a central ring that can be modulate in size (Table 1; Figure 2), namely 1,4-dihydropyrazolo[3,4-*a*]pyrrolizines (**2a–h**), 4,5-dihydro-1*H*-pyrazolo[4,3-*g*]indolizines (**2i–l**), 1,4,5,6-tetrahydropyrazolo[3,4-*c*]pyrrolo[1,2-*a*]azepines (**2m–p**) that varied the carbamoyl unit with the Cl or CH_3 substituents on the pyrrole moiety. Such bioisosteric benzene/pyrrole replacement might give access to pharmaceutically interesting

TABLE 1 Structures and binding data for compounds **2a–p**

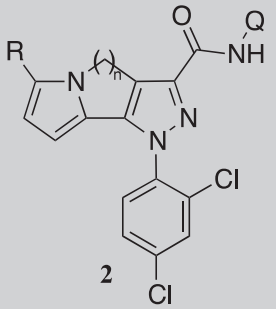

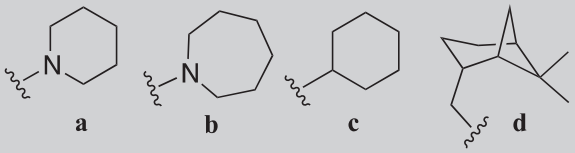

				Receptor affinity		CB_1 selectivity
Compound	**R**	***n***	**Q**	$K_i CB_1$ (nM)[a]	$K_i CB_2$ (nM)[b]	$K_i CB_2/K_i CB_1$
2a	Cl	1	**a**	902 ± 75	>1 μM	>1.10
2b	Cl	1	**b**	230 ± 36	615 ± 48	2.67
2c	Cl	1	**c**	715 ± 80	750 ± 66	1.05
2d	Cl	1	**d**	355 ± 39	314 ± 33	0.88
2e	CH_3	1	**a**	>1 μM	>1 μM	—
2f	CH_3	1	**b**	895 ± 70	>1 μM	>1.11
2g	CH_3	1	**c**	>1 μM	>1 μM	
2h	CH_3	1	**d**	142 ± 30	731 ± 75	5.15
2i	Cl	2	**a**	209 ± 25	>1 μM	>4.78
2j	Cl	2	**b**	81 ± 12	>1 μM	>12.35
2k	Cl	2	**c**	154 ± 22	>1 μM	>6.49
2l	Cl	2	**d**	>1 μM	>1 μM	—
2m	Cl	3	**a**	190 ± 30	>1 μM	>5.26
2n	Cl	3	**b**	244 ± 35	>1 μM	>4.10
2o	Cl	3	**c**	544 ± 48	958 ± 68	1.76
2p	Cl	3	**d**	257 ± 30	>1 μM	>3.89

[a]Affinity of compounds for the CB_1 receptor was evaluated using mouse whole-brain membranes and [^{3}H]CP 55940. K_i values were obtained from five independent experiments carried out in triplicate.

[b]Affinity of compounds for the CB_2 receptor was evaluated using CHO cell membranes transfected with hCB_2 receptors and [^{3}H]CP 55940. K_i values were obtained from five independent experiments carried out in triplicate.

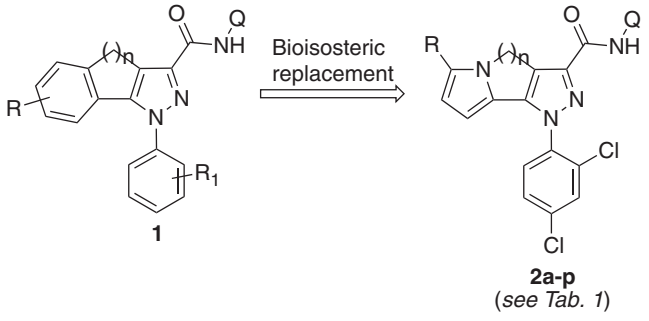

FIGURE 2 Design of CBR ligands by bioisosteric replacement benzene/pyrrole

compounds with modified physical–chemical properties, because the introduction of the pyrrole ring makes the tricyclic system more electron-rich. Moreover, it increases the polar surface area and decreases the lipophilicity.

In this article, we report the synthesis of compounds **2a–p** together with preliminary aspects of their affinity and selectivity on CBRs and molecular modelling studies. These data are accompanied by a thorough in silico evaluation of the pharmacokinetic properties, with the aim at gaining preliminary information concerning their potentially drug-like profile.

2 | MATERIALS AND METHODS

2.1 | Chemistry

2.1.1 | General

Melting points were obtained on a Koffler melting point apparatus and are uncorrected. IR spectra were recorded as Nujol mulls on NaCl plates with a Jasco FT/IR 460 plus

spectrophotometer and are expressed in ν (cm^{-1}). NMR experiments were run on a Bruker AVANCE III Nanobody 400 MHz spectrometer with ^{1}H and ^{13}C being observed at 400 and 100.6 MHz, respectively. Spectra were acquired using $CDCl_3$ as solvent. Chemical shifts for ^{1}H and ^{13}C NMR spectra were reported in δ (ppm) downfield from tetramethylsilane, and coupling constants (*J*) were expressed in Hertz. Multiplicities are recorded as s (singlet), d (doublet), t (triplet), dd (doublet of doublets), m (multiplet). Specific rotation was recorded with a PerkinElmer 241 apparatus, using the sodium D line (589 nm), and $CHCl_3$ as solvent. Atmospheric pressure ionization electrospray (API-ES) mass spectra were obtained on an Agilent 1100 series LC/MSD spectrometer. Elemental analyses were performed with a PerkinElmer 2400 analyser, and results were within ±0.40% of the calculated values. TLC was performed on Merck silica gel 60 TLC plates F254 and visualized using UV. Flash chromatography (FC) was performed using Merck silica gel 60 (230–400 mesh ASTM).

Chemical intermediates **3–18** and final compounds **2a**, **2e**, **2i** and **2m** (Table 1; Scheme 1) were synthesized according to literature procedure.[23] 1-Aminohomopiperidine, cyclohexylamine and (−)-*cis*-myrtanylamine were purchased from Sigma-Aldrich®.

2.1.2 | General procedure for the amidation of 15–18

1-(3-Dimethylaminopropyl)-3-ethylcarbodiimide (EDC) (1.2 mmol) and 1-hydroxybenzotriazole (HOBt) (1.2 mmol) were added in sequence to a suspension of the appropriate tricyclic acid (1 mmol) in CH_2Cl_2 (15 ml). After 1 hr, the suspension became a solution and then the appropriate amine (2 mmol) was added and stirring was continued at room temperature overnight. The organic phase was washed with water, dried over anhydrous Na_2SO_4 and concentrated under reduced pressure. The residue was purified by FC using the appropriate eluents.

6-Chloro-1-(2,4-dichlorophenyl)-*N*-(homopiperidin-1-yl)-1,4-dihydropyrazolo[3,4-*a*]pyrrolizine-3-carboxamide (2b)

Compound **2b** was obtained from **16** and 1-aminohomopiperidine. The crude residue was purified by FC (AcOEt/petroleum ether 3/7) to afford **2b** (0.29 g, 63%) as yellow solid; R_f 0.25 (AcOEt/petroleum ether 2/8); m.p. 167–168°C. IR 1,645 (C=O). ^{1}H NMR 7.62 (s, 1H), 7.53 (d, $J = 8.6$ Hz, 1H), 7.42 (d, $J = 8.6$ Hz, 1H), 7.40–7.30 (m, 1H), 6.09 (d, $J = 3.6$ Hz, 1H), 5.92 (d, $J = 3.6$ Hz, 1H), 4.89 (s, 2H), 3.30–3.00 (m, 4H), 1.90–1.50 (m, 8H). ^{13}C NMR 160.1, 141.9, 135.7, 130.8, 129.3, 128.0, 125.3, 124.7, 116.2, 109.3, 100.7, 58.6, 44.0, 27.0, 26.1. API-ES m/z: $[M + H]^+$ calcd for $C_{21}H_{21}Cl_3N_5O$: 464.1, found: 464.1. Anal. ($C_{21}H_{20}Cl_3N_5O$) C, H, N.

6-Chloro-1-(2,4-dichlorophenyl)-*N*-(cyclohexyl-1-yl)-1,4-dihydropyrazolo[3,4-*a*]pyrrolizine-3-carboxamide (2c)

Compound **2c** was obtained from **16** and cyclohexylamine. The crude residue was purified by FC (AcOEt/petroleum ether 15/85) to afford **2c** (0.29 g, 65%) as light brown solid; R_f 0.61 (AcOEt/petroleum ether 2/8); m.p. 194–196°C. IR

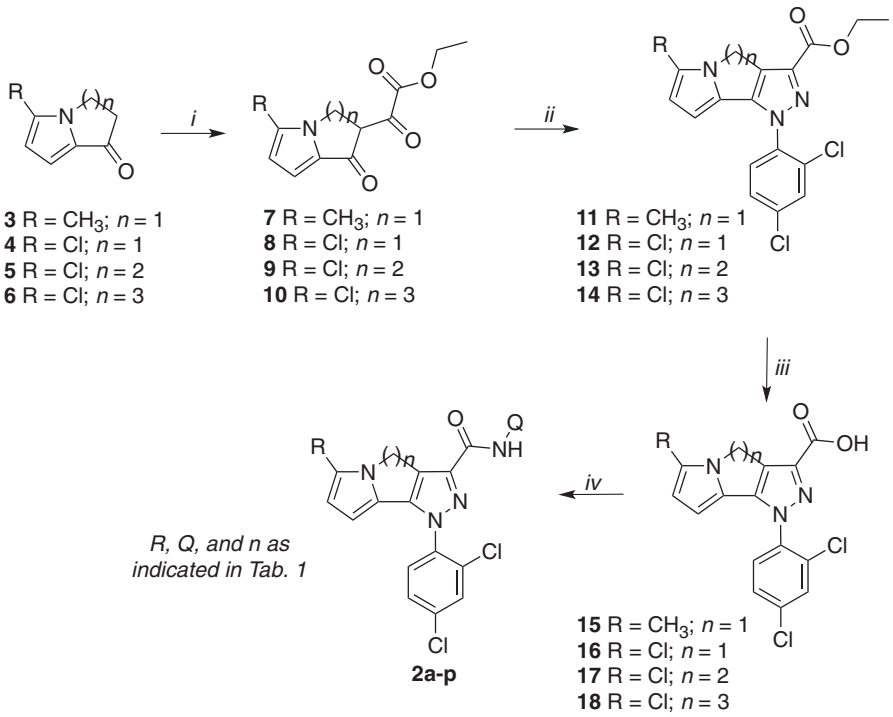

SCHEME 1 Reagents and conditions: (i) Na, EtOH, $(COOEt)_2$, r.t., 1 hr; (ii) 2,4-$Cl_2C_6H_3NHNH_2$·HCl, EtOH, 80°C, 8 hr; (iii) THF, LiOH 0.8 M, 60°C, 3 hr; (iv) EDC, HOBt, CH_2Cl_2, r.t., 1 hr, then NH_2-Q, overnight

1,645 (C=O). ^{1}H NMR 7.62 (s, 1H), 7.53 (d, J = 8.0 Hz, 1H), 7.42 (d, J = 8.0 Hz, 1H), 6.76 (d, J = 7.6 Hz, 1H), 6.08 (d, J = 2.8 Hz, 1H), 5.92 (d, J = 2.8 Hz, 1H), 4.91 (s, 2H), 4.08–3.78 (m, 1H), 2.15–1.88 (m, 2H), 1.88–1.71 (m, 2H), 1.71–1.50 (m, 1H), 1.50–1.34 (m, 2H), 1.36–1.10 (m, 3H). ^{13}C NMR 160.2, 141.9, 135.9, 130.8, 129.1, 128.3, 125.3, 124.7, 116.1, 109.4, 100.7, 48.3, 45.6, 33.3, 25.7, 25.1. API-ES m/z: $[M + H]^+$ calcd for $C_{21}H_{20}Cl_3N_4O$: 449.1, found: 449.2. Anal. ($C_{21}H_{19}Cl_3N_4O$) C, H, N.

6-Chloro-1-(2,4-dichlorophenyl)-*N*-(*cis*-myrtanyl-1-yl)-1,4-dihydropyrazolo[3,4-*a*]pyrrolizine-3-carboxamide (2d)

Compound **2d** was obtained from **16** and (−)-*cis*-myrtanylamine. The crude residue was purified by FC (AcOEt/petroleum ether 15/85) to afford **2d** (0.28 g, 55%) as light brown solid; m.p. 250–253°C; R_f 0.55 (AcOEt/petroleum ether 2/8). IR 1,645 (C=O). ^{1}H NMR 7.72 (s, 1H), 7.53 (d, J = 8.8 Hz, 1H), 7.43 (d, J = 8.8 Hz, 1H), 7.00–6.85 (m, 1H), 6.08 (d, J = 4.0 Hz, 1H), 5.92 (d, J = 4.0 Hz, 1H), 4.91 (s, 2H), 3.46–3.29 (m, 2H), 2.42–2.11 (m, 2H), 2.00–1.40 (m, 6H), 1.20 (s, 3H), 1.08 (s, 3H), 0.90 (d, J = 9.6 Hz, 1H). ^{13}C NMR 160.3, 142.5, 141.6, 135.7, 130.8, 130.2, 129.1, 128.7, 128.3, 125.0, 124.7, 116.1, 109.3, 100.9, 44.9, 44.8, 44.1, 41.7, 41.5, 38.9, 33.6, 28.0, 26.1, 23.4, 20.3. $[\alpha]_D$ −2.41 (*c* 0.1678, $CHCl_3$). API-ES m/z: $[M + H]^+$ calcd for $C_{25}H_{26}Cl_3N_4O$: 503.1, found: 503.2. Anal. ($C_{25}H_{25}Cl_3N_4O$) C, H, N.

6-Methyl-1-(2,4-dichlorophenyl)-*N*-(homopiperidin-1-yl)-1,4-dihydropyrazolo[3,4-*a*]pyrrolizine-3-carboxamide (2f)

Compound **2f** was obtained from **15** and 1-aminohomopiperidine. The crude residue was purified by FC (AcOEt/petroleum ether 3/7) to afford **2f** (0.20 g, 45%) as white solid; R_f 0.25 (AcOEt/petroleum ether 2/8); m.p. 154–155°C. IR 1,648 (C=O). ^{1}H NMR 8.26 (s, 1H), 7.61 (s, 1H), 7.52 (d, J = 8.1 Hz, 1H), 7.41 (d, J = 8.1 Hz, 1H), 5.98–5.91 (m, 1H), 5.92–5.81 (m, 1H), 4.82 (s, 2H), 3.35–3.03 (m, 4H), 2.27 (s, 3H), 1.87–1.77 (m, 4H), 1.73–1.61 (m, 4H). ^{13}C NMR 158.9, 145.4, 135.7, 135.6, 130.6, 129.3, 128.8, 128.1, 125.1, 124.9, 124.8, 109.6, 99.9, 58.5, 44.4, 26.9, 26.0, 11.9. API-ES m/z: $[M + H]^+$ calcd for $C_{22}H_{24}Cl_2N_5O$: 444.1, found: 444.2. Anal. ($C_{22}H_{23}Cl_2N_5O$) C, H, N.

6-Methyl-1-(2,4-dichlorophenyl)-*N*-(cyclohexyl-1-yl)-1,4-dihydropyrazolo[3,4-*a*]pyrrolizine-3-carboxamide (2g)

Compound **2g** was obtained from **15** and cyclohexylamine. The crude residue was purified by FC (AcOEt/petroleum ether 15/85) to afford **2g** (0.21 g, 49%) as white solid; R_f 0.60 (AcOEt/petroleum ether 2/8); m.p. 130–133°C. IR 1,653 (C=O). ^{1}H NMR 7.61 (d, J = 1.6 Hz, 1H), 7.53 (d, J = 8.6 Hz, 1H), 7.41 (dd, J = 8.6, 1.6 Hz, 1H), 6.80 (d, J = 8.0 Hz, 1H), 5.94 (d, J = 3.0 Hz, 1H), 5.88 (d, J = 3.0 Hz, 1H), 4.83 (s, 2H), 4.04–3.84 (m, 1H), 2.27 (s, 3H), 2.07–1.97 (m, 2H), 1.80–1.72 (m, 2H), 1.68–1.58 (m, 1H), 1.50–1.35 (m, 2H), 1.35–1.03 (m, 3H). ^{13}C NMR 160.5, 145.5, 142.0, 135.9, 135.7, 130.8, 130.7, 129.4, 129.0, 128.2, 125.1, 125.0, 109.6, 99.9, 48.3, 44.6, 33.3, 25.7, 25.1, 12.0. API-ES m/z: $[M + H]^+$ calcd for $C_{22}H_{23}Cl_2N_4O$: 429.1, found: 429.0. Anal. ($C_{22}H_{22}Cl_2N_4O$) C, H, N.

6-Methyl-1-(2,4-dichlorophenyl)-*N*-(cis-myrtanyl-1-yl)-1,4-dihydropyrazolo[3,4-*a*]pyrrolizine-3-carboxamide (2h)

Compound **2h** was obtained from **15** and (−)-*cis*-myrtanylamine. The crude residue was purified by FC (AcOEt/petroleum ether 15/85) to afford **2h** (0.17 g, 35%) as white solid; R_f 0.62 (AcOEt/petroleum ether 2/8); m.p. 178–179°C; IR 1,651 (CO). ^{1}H NMR 7.62 (d, J = 2.0 Hz, 1H), 7.53 (d, J = 8.6 Hz, 1H), 7.41 (dd, J = 8.6, 2.0 Hz, 1H), 6.98 (t, J = 6.0 Hz, 1H), 5.94 (d, J = 3.6 Hz, 1H), 5.88 (d, J = 3.6 Hz, 1H), 4.84 (s, 2H), 3.56–3.33 (m, 2H), 2.40–2.29 (m, 2H), 2.27 (s, 3H), 2.03–1.96 (m, 2H), 1.96–1.81 (m, 3H), 1.64–1.51 (m, 1H), 1.21 (s, 3H), 1.09 (s, 3H), 0.91 (d, J = 9.6 Hz, 1H). ^{13}C NMR 161.5, 145.6, 141.8, 135.9, 135.7, 130.9, 130.8, 129.4, 128.9, 128.2, 125.2, 124.9, 109.6, 99.9, 44.9, 44.7, 43.9, 41.7, 41.5, 38.9, 33.4, 28.1, 26.2, 23.4, 20.0, 12.0. $[\alpha]_D$ −3.08 (*c* 0.2048, $CHCl_3$). API-ES m/z: $[M + H]^+$ calcd for $C_{26}H_{29}Cl_2N_4O$: 483.2, found: 483.3. Anal. ($C_{26}H_{28}Cl_2N_4O$) C, H, N.

7-Chloro-1-(2,4-dichlorophenyl)-*N*-(homopiperidin-1-yl)-4,5-dihydro-*1H*-pyrazolo[4,3-*g*]indolizine-3-carboxamide (2j)

Compound **2j** was obtained from **17** and 1-aminohomopiperidine. The crude residue was purified by FC (AcOEt/petroleum ether 3/7) to afford **2j** (0.17 g, 36%) as white solid; R_f 0.28 (AcOEt/petroleum ether 2/8); m.p. 150–152°C. IR 1,645 (C=O). ^{1}H NMR 8.01 (s, 1H), 7.63 (s, 1H), 7.46–7.38 (m, 2H), 5.93 (d, J = 3.8 Hz, 1H), 5.41 (d, J = 3.8 Hz, 1H), 4.10 (t, J = 6.8 Hz, 2H), 3.39 (t, J = 6.8 Hz, 2H), 3.14 (t, J = 5.6 Hz, 4H), 1.80–1.45 (m, 8H). ^{13}C NMR 161.5, 143.6, 137.1, 136.8, 136.2, 133.9, 130.7, 130.6, 128.3, 120.7, 119.1, 112.7, 107.2, 104.4, 58.5, 42.3, 26.9, 26.0, 20.7. API-ES m/z: $[M + H]^+$ calcd for $C_{22}H_{23}Cl_3N_5O$: 478.1, found: 478.0. Anal. ($C_{22}H_{22}Cl_3N_5O$) C, H, N.

7-Chloro-1-(2,4-dichlorophenyl)-*N*-(cyclohexyl-1-yl)-4,5-dihydro-*1H*-pyrazolo[4,3-*g*]indolizine-3-carboxamide (2k)

Compound **2k** was obtained from **17** and cyclohexylamine. The crude residue was purified by FC (AcOEt/petroleum ether 15/85) to afford **2k** (0.18 g, 40%) as light brown solid R_f 0.55 (AcOEt/petroleum ether 2/8); m.p. 190–192°C. IR 1,650

(C=O). ^{1}H NMR 7.62 (s, 1H), 7.44 (s, 2H), 6.85–6.58 (m, 1H), 5.94 (d, J = 4.0 Hz, 1H), 5.40 (d, J = 4.0 Hz, 1H), 4.10 (d, J = 6.8 Hz, 2H), 4.01–3.84 (m, 1H), 3.40 (d, J = 6.8 Hz, 2H), 2.01 (d, J = 12.0 Hz, 2H), 1.82–1.66 (m, 2H), 1.68–1.60 (m, 1H), 1.46–1.12 (m, 5H). ^{13}C NMR 161.5, 143.6, 137.0, 136.9, 136.0, 133.8, 130.7, 130.5, 128.3, 120.7, 119.0, 112.7, 107.2, 104.4, 48.2, 42.3, 33.3, 25.7, 25.1, 20.9. API-ES m/z: $[M + H]^+$ calcd for $C_{22}H_{22}Cl_3N_4O$: 463.1, found: 463.2. Anal ($C_{22}H_{21}Cl_3N_4O$) C, H, N.

7-Chloro-1-(2,4-dichlorophenyl)-*N*-(*cis*-myrtanyl-1-yl)-4,5-dihydro-*1H*-pyrazolo[4,3-*g*]indolizine-3-carboxamide (2l)

Compound **2l** was obtained from **17** and (−)-*cis*-myrtanylamine. The crude residue was purified by FC (AcOEt/petroleum ether 15/85) to afford **2l** (0.31 g, 61%) as light brown solid; R_f 0.60 (AcOEt/petroleum ether 2/8); m.p. 192–193°C. IR 1,645 (C=O). ^{1}H NMR 7.63 (s, 1H), 7.45 (s, 2H), 7.00–6.80 (m, 1H), 5.95 (d, J = 3.0 Hz, 1H), 5.41 (d, J = 3.0 Hz, 1H), 4.10 (t, J = 7.0 Hz, 2H), 3.40 (t, J = 7.0, 2H), 3.50–3.31 (m, 2H), 2.41–2.23 (m, 2H), 2.01–1.84 (m, 5H), 1.73–1.52 (m, 1H), 1.20 (m, 3H), 1.07 (s, 3H), 1.00–0.80 (m, 1H). ^{13}C NMR 161.5, 143.6, 137.0, 136.9, 136.0, 133.8, 130.7, 130.5, 128.3, 120.7, 119.0, 112.7, 107.2, 104.4, 44.9, 44.5, 43.9, 41.5, 41.1, 38.6, 33.1, 28.7, 26.2, 23.4, 20.1. $[\alpha]_D$ −1.86 (*c* 0.20, $CHCl_3$). API-ES m/z: $[M + H]^+$ calcd for $C_{26}H_{28}Cl_3N_4O$: 517.1, found: 517.2. Anal. ($C_{26}H_{27}Cl_3N_4O$): C, H, N.

8-Chloro-1-(2,4-dichlorophenyl)-*N*-(homopiperidin-1-yl)-1,4,5,6-tetrahydropyrazolo[3,4-*c*]pyrrolo[1,2-*a*]azepine-3-carboxamide (2n)

Compound **2n** was obtained from **18** and homopiperidine. The crude residue was purified by FC (AcOEt/petroleum ether 3/7) to afford **2n** (0.20 g, 40%) as pink solid; R_f 0.21 (AcOEt/petroleum ether 2/8); m.p. 160–162°C. IR 1,645 (C=O). ^{1}H NMR 8.04 (s, 1H), 7.54 (s, 1H), 7.46–7.35 (m, 2H), 5.89 (d, J = 3.8 Hz, 1H,), 5.33 (d, J = 3.8 Hz, 1H,), 4.20–4.05 (m, 2H), 3.40–3.20 (m, 3H), 3.19–3.05 (m, 3H), 2.31–2.22 (m, 2H), 1.82–1.54 (m, 8H). ^{13}C NMR (101 MHz, $CDCl_3$) 163.2, 146.5, 136.2, 135.9, 133.9, 133.6, 130.7, 130.4, 128.2, 121.8, 117.9, 116.4, 108.4, 106.9, 58.3, 44.7, 26.9, 26.2, 23.9. API-ES m/z: $[M + H]^+$ calcd for $C_{23}H_{25}Cl_3N_5O$: 492.1, found: 492.2. Anal. ($C_{23}H_{24}Cl_3N_5O$) C, H, N.

8-Chloro-1-(2,4-dichlorophenyl)-*N*-(cyclohexyl-1-yl)-1,4,5,6-tetrahydropyrazolo[3,4-*c*]pyrrolo[1,2-*a*]azepine-3-carboxamide (2o)

Compound **2o** was obtained from **18** and cyclohexylamine. The crude residue was purified by FC (AcOEt/petroleum ether 15/85) to afford **2o** (0.20 g, 42%) as pink solid; R_f 0.21 (AcOEt/petroleum ether 1/1); m.p. 150–152°C. IR 1,645 (C=O). ^{1}H NMR 7.53 (s, 1H), 7.41 (s, 2H), 6.83 (d, J = 7.6 Hz, 1H), 5.89 (d, J = 2.4 Hz, 1H), 5.33 (d, J = 2.4 Hz, 1H), 4.20–4.05 (m, 2H), 4.00–3.83 (m, 1H), 3.42–3.24 (m, 2H), 2.24–2.10 (m, 2H), 2.10–1.88 (m, 2H), 1.87–1.50 (m, 4H), 1.44–1.36 (m, 4H). ^{13}C NMR: 163.2, 146.5, 136.2, 135.9, 133.7, 133.6, 130.7, 130.4, 128.2, 121.8, 117.9, 116.4, 108.4, 106.9, 48.3, 44.7, 44.6, 33.3, 26.9, 25.7, 24.0, 25.1. API-ES m/z: $[M + H]^+$ calcd for $C_{23}H_{24}Cl_3N_4O$: 477.1, found: 477.0. Anal. ($C_{23}H_{23}Cl_3N_4O$): C, H, N.

8-Chloro-1-(2,4-dichlorophenyl)-*N*-(*cis*-myrtanyl-1-yl)-1,4,5,6-tetrahydropyrazolo[3,4-*c*]pyrrolo[1,2-*a*]azepine-3-carboxamide (2p)

Compound **2p** was obtained from **18** and (−)-*cis*-myrtanylamine. The crude residue was purified by FC (AcOEt/petroleum ether 15/85) to afford **2p** (0.16 g, 30%) as light brown solid; R_f 0.68 (AcOEt/petroleum ether 2/8); m.p. 154–155°C. IR 1,645 (C=O). ^{1}H NMR 7.53 (s, 1H), 7.42–7.30 (m, 2H), 7.10–6.90 (m, 1H), 5.89 (s, 1H), 5.34 (s, 1H), 4.23–4.05 (m, 2H), 3.44–3.23 (m, 2H), 3.10–3.02 (m, 2H), 2.41–2.10 (m, 4H), 2.00–1.88 (m, 2H), 1.88–1.76 (m, 3H), 1.60–1.48 (m, 1H), 1.19 (s, 3H), 1.07 (s, 3H), 0.80–1.00 (m, 1H). ^{13}C NMR 163.1, 146.5, 136.4, 136.1, 133.8, 133.6, 130.7, 130.5, 128.5, 121.8, 118.0, 116.4, 108.3, 107.1, 44.7, 44.2, 44.1, 42.0, 41.4, 38.8, 33.4, 28.2, 26.1, 26.0, 24.0, 23.5, 20.3. $[\alpha]_D$ −2.10 (*c* 0.2017, $CHCl_3$). API-ES m/z: $[M + H]^+$ calcd for $C_{27}H_{30}Cl_3N_4O$: 531.1, found: 531.2. Anal. ($C_{27}H_{29}Cl_3N_4O$) C, H, N.

2.2 | Biological assays

2.2.1 | Radioligand-binding assays

General procedures binding experiments

Affinities at CB_1R and CB_2R for **2a–p** were assessed by competition for [^{3}H]CP-55940 binding in mouse whole-brain membranes and Chinese hamster ovary (CHO) cell membranes transfected with hCB_2, respectively.[24]

Mouse brain membranes[25]

Whole-mouse brains from four adult male MF1 mice were suspended in centrifugation buffer (320 mM sucrose, 2 mM Tris–HCl, 2 mM Tris base, 2 mM EDTA, 5 mM $MgCl_2$ at pH 7.4) and the tissue homogenized with an Ultra-Turrex homogenizer. Tissue homogenates were centrifuged at 1,600 *g* for 10 min and the resulting supernatant collected. The pellet was resuspended in centrifugation buffer, centrifuged as before and the supernatant collected. Supernatants were combined before undergoing further centrifugation at 28,000 *g* for 20 min. The supernatant was discarded and the pellet resuspended in 20 ml of buffer A (50 mM Tris–HCl, 50 mM Tris base, 2 mM EDTA, 5 mM $MgCl_2$ at pH 7.0) and incubated at 37°C for 10 min. Following the incubation, the suspension

was centrifuged for 20 min at 23,000 *g*. After resuspending the pellet in another 20 ml of buffer A, the suspension was incubated for 40 min at room temperature before a final centrifugation for 15 min at 11,000 *g*. The final pellet was resuspended in 2 ml of buffer B (50 mM Tris–HCl, 50 mM Tris base, 1 mM EDTA, 3 mM $MgCl_2$ at pH 7.4) to give a protein concentration of 1 mg/ml and stored at 80°C. All centrifugation procedures were carried out at 4°C.

CHO cell membranes[24]

CHO cells stably transfected with cDNA encoding human cannabinoid CB_2R (Bmax = 72.6 pmol/mg protein) were maintained at 37°C and 5% CO_2 in Dulbecco's modified Eagle's medium (DMEM) nutrient mixture F-12 HAM supplemented with 10% foetal bovine serum (FBS), 3 ml penicillin–streptomycin and 4 ml G-418. These CHO hCB_2 cells were passed twice a week using a nonenzymatic cell dissociation solution (5 ml EDTA). The hCB_2-transfected cells were removed from flasks by scraping and then frozen as a pellet at −20°C until required. Before use in a radioligand-binding assay, cells were defrosted, diluted in 50 mM Tris-binding buffer (see radioligand displacement assay) and homogenized with a 1 ml hand-held homogenizer. Protein assays were performed using a Bio-Rad Dc kit.

Radioligand competition assay[24]

Binding experiments were carried out with [^{3}H]CP-55940, Tris-binding buffer (50 mM Tris–HCl, 50 mM Tris base; 0.1% BSA, pH 7.4), total assay volume 500 ml, using the filtration procedure described previously by Ross et al.[19] Binding was initiated by the addition of mouse brain (CB_1 assay) or CHO cells (CB_2 assay) membranes (50 μg protein per tube). All assays were performed at 37°C for 60 min before termination by addition of ice-cold Tris-binding buffer and vacuum filtration using a 12-well sampling manifold (Cell Harvester; Brandel) and Whatman GF/B glass-fibre filters that had been soaked in wash buffer at 4°C for 24 hr. Each reaction tube was washed five times with the wash buffer. The filters were oven-dried for 60 min and then placed in 5 ml of scintillation fluid. Radioactivity was quantified by liquid scintillation spectrometry. *Specific binding* was defined as the difference between the binding that occurred in the presence and absence of 1 μM unlabelled CP-55940. The concentration of [^{3}H]CP-55940 used in our displacement assays was 0.7 nM. Each unlabelled cannabinoid tested was stored as a stock solution of 10 mM in DMSO, the vehicle concentration in all assay tubes being 0.1% DMSO. Protein assays were performed using a Bio-Rad Dc kit. The binding parameters for [^{3}H]CP-55940, determined by fitting data from saturation-binding experiments to a one-site saturation plot using GraphPad Prism, were 2,336 fmol/mg protein (Bmax) and 2.31 nM (Kd) in mouse brain membranes and 72,570 fmol/mg protein (Bmax) and 4.3 nM (Kd) in hCB_2-transfected cells.

2.3 | Molecular modelling

2.3.1 | Ligand preparation and docking studies

All the compounds were built, parameterized (Gasteiger–Huckel method) and energy minimized within MOE using MMFF94 forcefield.[1]

Docking calculations within the X-ray structure of the CB_1R (pdb code = 5TGZ; resolution = 2.8 Å)[26] were performed using the LEADIT 2.1.8 software suite.[2] This tool includes the FlexX scoring algorithm, which is based on calculation of the binding free energy by means of Gibbs–Helmholtz equation.[27] The software detects the binding site defining a radius of 10 Å far from the co-crystallized ligand, to set up a spherical search space for the docking approach.

The standard setting as docking strategy was followed, choosing the so-called Hybrid Approach (enthalpy and entropy criteria), the related scoring function evaluation is described in the literature.[28] The derived docking poses were prioritized taking into account the score values of the lowest energy pose of the compounds docked to the protein structure. All ligands were further refined and rescored by assessment with the algorithm HYDE, included in the LEADIT 2.1.8 software. The HYDE module considers dehydration enthalpy and hydrogen bonding.[29]

Then, the stability of the selected protein–ligand complexes was assessed using a short ~1 ps run of molecular dynamics (MD) at constant temperature, followed by an all-atom energy minimization (LowModeMD implemented in MOE software). This kind of module allowed to perform an exhaustive conformational analysis of the ligand–receptor binding site subset, as we previously reported about other case studies.[22e,30]

2.3.2 | In silico evaluation of pharmacokinetic properties

The prediction of ADMET properties was performed using the Advanced Chemistry Development (ACD) Percepta platform (www.acdlabs.com).

Any ADMET descriptor was evaluated by Percepta based on training libraries implemented in the software, which includes a consistent pool of molecules whose pharmacokinetic and toxicity profiles are experimentally known.

TPSA descriptor, representing the polar surface area ($Å^2$) of the molecules, was evaluated by means of MOE software. TPSA is calculated using group contributions to approximate

the polar surface area from connection table information only. The parameterization is that of Ertl et al.[31]

3 | RESULTS AND DISCUSSION

3.1 | Chemistry

The strategy followed for pyrrolocycloalkylpyrazole-based compounds **2** is outlined in Scheme 1 and started with substituted pyrrolocycloalkanones **3–6**.[23] Ketones were first transformed to **7–10** using a Claisen reaction and next condensed with 2,4-dichlorophenylhydrazine to give the tricyclic pyrrolocycloalkylpyrazoles **11–14**. Final elaboration to designed compounds **2a–p** was accomplished by functional interconversion of esters **11–14** via acid **15–18** to the amides/hydrazides.

3.2 | Cannabinoid receptor binding studies

Affinities at CB_1R and CB_2R for compounds **2** were assessed by competition for [^{3}H]CP-55940 binding in mouse whole-brain membranes and Chinese hamster ovary (CHO) cell membranes transfected with hCB_2, respectively. The experimental data (IC_{50} values) were converted into K_i values[32] and are shown in Table 1.

To investigate how bioisosteric replacement benzene/pyrrole can modify binding profile of the tricyclic scaffold, three series of tricyclic pyrrolopyrazoles **2a–p** structurally correlated to compounds **1Aa**, **1Ab**, **1B** and **1C**, were synthesized. Any of the new synthesized compounds showed high affinity for CB_2R with K_i values superior to 314 nM, whereas some of them showed moderate affinity for CB_1R with K_i values inferior to 400 nM.

The 1,4-dihydropyrazolo[3,4-*a*]pyrrolizine compounds **2a–d** with a chlorine atom at C_5 showed moderate binding affinity to CB_1R and values that were from 314 nM to >1 μM range for CB_2R subtype. The highest affinity for both CBRs was shown by the ligand bearing the homopiperazine carbamoyl unit. Compound **2b**, the best of this group with a CB_1R affinity of 230 nM and CB_2R affinity of 615 nM, was used as reference term for all of the others to present SAR studies. Compound **2a**, having a piperazine ring replacement of the homopiperazine ring of the carbamoyl unit, showed much lower affinity for CB_1R as compared to **2b** and no significant affinity for CB_2R (K_i > 1 μM). Compound **2c** with a cyclohexyl moiety in the carbamoyl unit exhibited little change in binding affinity between CBRs, however, resulting in a threefold to 1.2-fold reduction. Compound **2d**, in which the size and shape of amine unit were markedly changed by introduction of the myrtanyl moiety, showed a slight increase of CB_2R affinity (K_i 314 nM) and decrease in CB_1R affinity (K_i 355 nM) with K_1CB_2/K_iCB_1 values lying in the same order of magnitude with respect to compound **2b**. Changing the chlorine atom on the pyrrole ring of the 1,4-dihydropyrazolopyrrolizine scaffold with a methyl group, compounds **2e–h**, showed a quite negative impact on CBRs affinity, with the exception of compound **2h**. The myrtanyl derivative **2h** had the highest CBRs affinity among the four methyl substituted analogues with a CB_1R affinity that is 1,6-fold higher to that of **2b**. CB_2R affinity of **2h** mirrored the ground term **2b**. Therefore, within the subseries **2e–h**, the introduction of bulky hydrophobic myrtanyl unit proved to be suitable for CB_2R interaction, resulting in a slight improvement of CB_2/CB_1 selectivity ratio with respect to **2b**. However, compound **2h** and all pyrrolizine analogues presented in this study did not reach the interesting binding profile exhibited by reference compounds **1Aa** and **1Ab** (Figure 1), indicating that the bioisosteric replacement benzene/pyrrole has a negative impact on CBR affinity.

The 4,5-dihydro-1*H*-pyrazolo[4,3-*g*]indolizines **2i–l** had higher CB_1R affinity with the only exception of **2l** as compared to **2b**. By contrast, ligands **2i–l** showed no binding preference for CB_2R. Among these derivatives, the homopiperidine substituent analogue, **2j**, had a good affinity for CB_1R (K_iCB_1 = 81 nM) together with the highest CB_2/CB_1 selectively ratio (>12).

The 1,4,5,6-tetrahydropyrazolo[3,4-*c*]pyrrolo[1,2-*a*]azepines **2m–p** displayed a similar pattern of binding to CBR affinities and no significant CB_2R affinity. Among these derivatives, the piperidine substituted analogue **2m** exhibited moderate affinity for CB_1R with a K_i value similar to that of **2b**.

According to these SAR studies based on three main series of compounds characterized by five, six and seven atoms in the central ring of the condensed tricyclic pyrrolopyrazole system, the planar dihydropyrazolo[3,4-*a*]pyrrolizine architecture appeared an important feature to assure moderate CB_1/CB_2R affinity. By contrast, the enlargement of the size of the central ring in the condensed tricyclic scaffold engenders conformational changes that promote the affinity for CB_1R and improve the CB_2/CB_1 selectivity ratio (*vide infra*, molecular modelling section).

3.3 | Molecular modelling

Nowadays, the rational design and discovery of CB_1 ligands were efficiently driven by deepening computational studies, including homology modelling of the biological target,[33] as well as ligand-based analyses.[34] The recent X-ray crystallographic structures of the cannabinoid CB_1R became available (pdb code = 5U09; resolution = 2.6 Å),[35] (pdb code = 5TGZ; resolution = 2.8 Å),[26] providing useful guidelines for the rational design of novel derivatives. These experimental data disclosed the binding mode of the co-crystallized propanamide-based (pdb code = 5U09) and

pyrazole-containing (pdb code = 5TGZ) derivatives, shedding light for the design of further series of analogues and/or isosteres.

In this work, we performed docking studies of the newly synthesized compounds, choosing as reference compound the pyrazole ligand (AM6538) co-crystallized in hCB_1 (pdb code = 5TGZ), because of the structural similarity to the derivatives here investigated (Figure 3; Table S1).

As shown in the following Figures 4–7, AM6538 exhibited one H-bond between the hydrogen atom of the carboxamide group and the side chain of S383, moving the piperidyl substituent towards I119, F174, A380, M384. The two aromatic centres occupied a deep hydrophobic pocket including I169, L193, V196, F268, W279, L359, W356, M363, L387. In this way, a number of Van der Waals contacts and π–π stacking were detected. Similarly, the well-known CB_1 antagonist rimonabant was able to display a highly comparable docking positioning if compared to the co-crystallized compound AM6538 (Figure 4).

Docking calculations on the newly synthesized molecules (**2a–2p**) allowed us to explore the putative binding mode exhibited by the cannabinoid ligands bearing the 1,4-dihydropyrazolo[3,4-*a*]pyrrolizines (**2a–h**), 4,5-dihydro-1*H*-pyrazolo[4,3-*g*]indolizines (**2i–l**) and the 1,4,5,6-tetrahydropyrazolo[3,4-*c*]pyrrolo[1,2-*a*]azepines (**2m–p**) containing derivatives within the human CB_1R. In particular, the SAR for the three series of compounds has been clarified, when the tricyclic core is coupled with hydrazide or carboxamide moieties as Q group.

Thus, all of them displayed a common positioning, moving the tricyclic core and the phenyl ring towards the two phenyl rings linked to the position 5 and to the position 1 of the pyrazole scaffold in AM6538, in order to gain the same hydrophobic contacts. On the other hand, the hydrazide or the carboxamide moieties exhibited a comparable docking mode, sometimes detecting H-bonds with S383. In particular, the presence of one acid hydrogen atom onto the nitrogen one of the carboxamide (or hydrazide) moiety resulted to be a key-feature for H-bonding S383 side chain, especially in presence of a bulky hydrophobic group in Q. Among the three series of compounds, the 4,5-dihydro-1*H*-pyrazolo[4,3-*g*]indolizine- and the 1,4,5,6-tetrahydropyrazolo[3,4-*c*]pyrrolo[1,2-*a*]azepine-containing derivatives were well suited and preferred to the 1,4-dihydropyrazolo[3,4-*a*]pyrrolizines. Indeed, compounds **2i–2p** moved the tricyclic core much more in proximity of the aforementioned phenyl ring of compound AM6538 (Figure 5, compound **2j** is shown, and Figure 6, compound **2n** is shown).

Conversely, the 1,4-dihydropyrazolo[3,4-*a*]pyrrolizine experienced a much more rigid conformation, leading the compound to quite differently accommodate within the human CB_1 binding site (Figure 7, compound **2b** is shown).

Notably, the improved CB_1-targeting ability occurring when the pyrrolizine scaffold (**2a–h**; hCB_1 = 142 nM to >1,000 μM) was modified to the indolizine core (**2i–l**; hCB_1 = 81 nM to >1,000 μM) and to the pyrroloazepine one (**2m–p**; hCB_1 = 190–544 nM) resembles the CB_1 affinity trend drawn by the bioisosteres 1,4-dihydroindeno[1,2-*c*]pyrazole

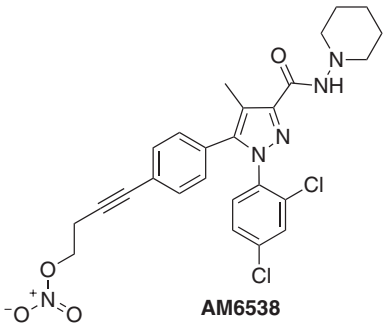

FIGURE 3 Chemical structure of pyrazole ligand AM6538

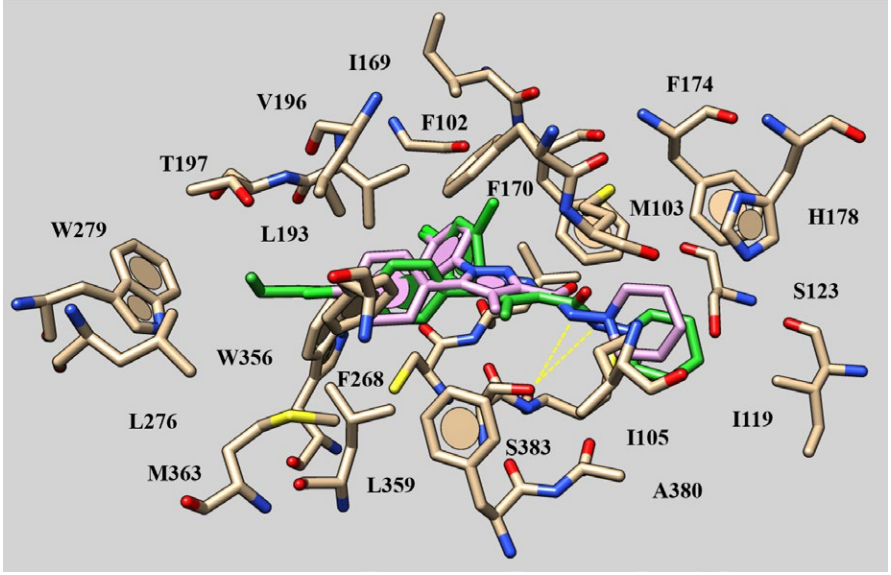

FIGURE 4 Docking mode of rimonabant (C atom; pink) within the X-ray crystallographic co-ordinates of hCB_1 receptor in complex with AM6538 (C atom; green). The most important residues are labelled. H-bonds detected by the two CB_1 antagonists are shown by dot lines (in yellow)

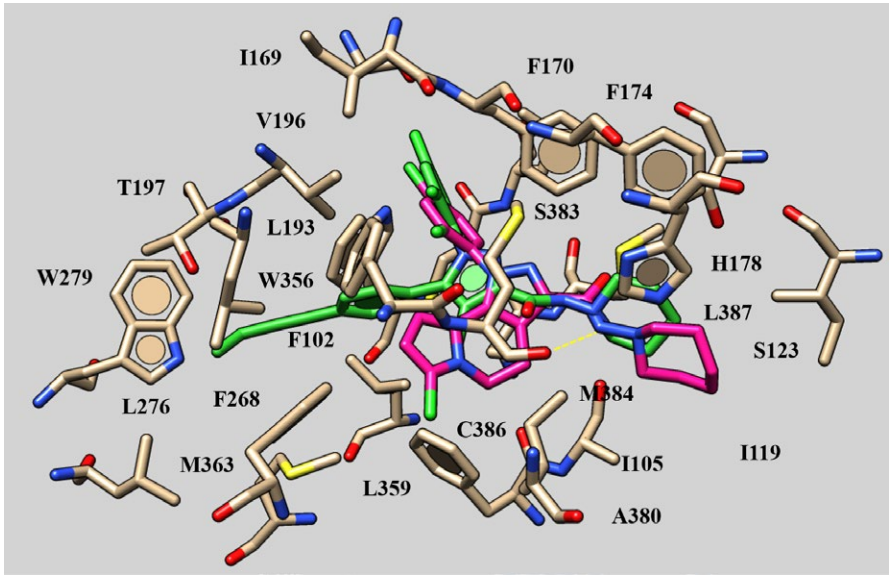

FIGURE 5 Docking mode of **2j** (C atom; magenta) within the X-ray crystallographic co-ordinates of hCB_1 receptor in complex with AM6538 (C atom; green). The most important residues are labelled. H-bonds detected by the 4,5-dihydro-1*H*-pyrazolo[4,3-*g*]indolizine compound are shown by dot lines (in yellow)

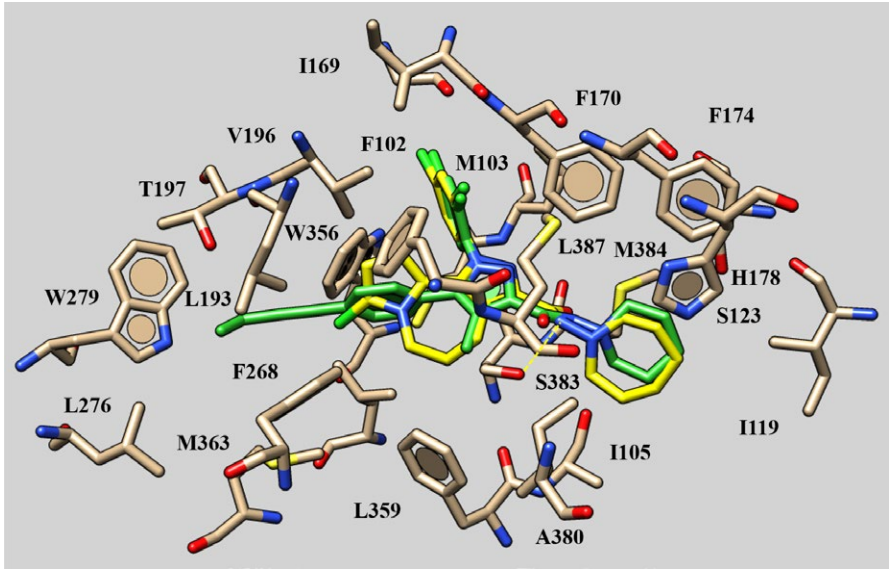

FIGURE 6 Docking mode of **2n** (C atom; yellow) within the X-ray crystallographic co-ordinates of hCB_1 receptor in complex with AM6538 (C atom; green). The most important residues are labelled. H-bonds detected by the 1,4,5,6-tetrahydropyrazolo[3,4-*c*] pyrrolo[1,2-*a*]azepine compound are shown by dot lines (in yellow)

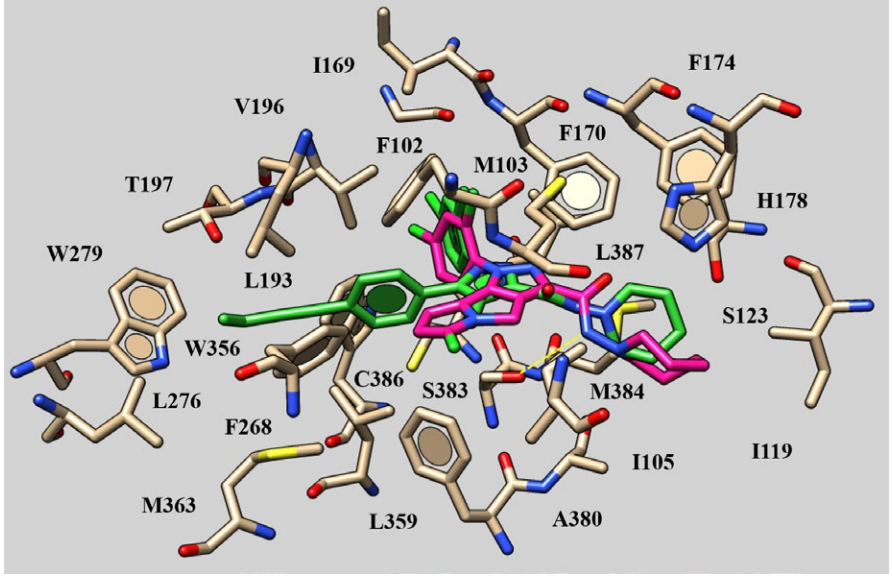

FIGURE 7 Docking mode of **2b** (C atom; magenta) within the X-ray crystallographic co-ordinates of hCB_1 receptor in complex with AM6538 (C atom; green). The most important residues are labelled. H-bonds detected by the 1,4-dihydropyrazolo[3,4-*a*]pyrrolizine compound are shown by dot lines (in yellow)

1Aa ($hCB_1 = 2050$ nM), 4,5-dihydro-1*H*-benzo[*g*]indazole **1B** ($hCB_1 = 14.8$ nM) and 1,4,5,6-tetrahydrobenzo[6,7]cyclohepta[1,2-*c*]pyrazole ligands **1C** ($hCB_1 = 4.2$ nM).

Nevertheless, based on a perspective of the docking results for all the three series of derivatives, adequate CB_1 antagonism could be achieved with the introduction of proper bulky hydrophobic groups in Q. Indeed, in any case, this substituent fall within a protein narrow cavity, delimited by I119, F174, A380, M384. Then, lipophilic cores, such as the cyclohexyl or myrtanyl moieties, proved to be the most suitable in simulate the binding mode of the co-crystallized ligand, making the compound promising in CB_1-targeting.

3.4 | In silico evaluation of pharmacokinetic properties

In the search of more druggable compounds, we deemed interesting to evaluate in silico the pharmacokinetic profile of the newly proposed derivatives, with respect to the prototypes **1Aa**, **1Ab**, **1B** and **1C**, by prediction of the most important descriptors related to absorption, blood–brain barrier (BBB) permeation and distribution. In details, we took into account the topological polar surface area (Å^2), the logarithmic ratio of the octanol–water partitioning coefficient (cLogP), extent of blood–brain barrier permeation (LogBB), rate of passive diffusion-permeability (LogPS), human intestinal absorption (HIA), volume of distribution (Vd), the role played by plasmatic protein binding (%PPB) and by the compound affinity towards the human serum albumin ($LogK_a^{HSA}$), and an overall perspective of the molecule oral bioavailability (%*F*).

As shown in Table 2, the bioisosteric replacement benzene/pyrrole experienced by **2a–p** led to compounds endowed with higher polar surface area and decreased lipophilicity. In particular, compounds **2a**, **2e**, **2i** and **2m** (TPSA = 55.09 Å^2; cLogP = 4.67–5.46) displayed higher TPSA and lower cLogP values if compared with the strictly related analogues **1Aa**,

TABLE 2 Calculated pharmacokinetic descriptors related to absorption and distribution properties

Compound	TPSA[a] (Å^2)	cLogP	LogBB[b]	LogPS[c]	HIA (%)[d]	Vd (L/kg)[e]	%PPB	pKa^{HSA}	%*F* (oral)
2a	55.09	5.02	0.47	−1.1	100	2.8	97.83	6.43	52.2
2b	55.09	5.47	0.72	−1.2	100	2.9	96.92	6.21	21.2
2c	51.85	6.20	0.60	−1.8	100	2.9	97.92	5.64	34.6
2d	51.85	7.51	0.23	−2.6	100	4.1	99.16	5.90	7.6
2e	55.09	4.67	0.57	−1.1	100	2.7	96.37	6.15	54.6
2f	55.09	5.15	0.83	−1.1	100	2.9	95.44	6.06	21.2
2g	51.85	5.79	0.63	−1.5	100	2.8	97.67	5.36	43.9
2h	51.85	7.25	0.46	−2.4	100	4.0	98.55	5.70	13.4
2i	55.09	5.26	0.01	−1.2	100	2.9	99.33	6.66	49.2
2j	55.09	5.69	0.01	−1.2	100	3.7	99.13	6.43	12.4
2k	51.85	6.45	0.10	−1.8	100	3.6	99.36	5.95	25.2
2l	51.85	7.77	−0.38	−2.7	100	4.5	99.75	6.05	4.4
2m	55.09	5.46	0.54	−1.2	100	3.0	97.96	5.61	90.0
2n	55.09	5.93	0.74	−1.3	100	3.8	97.07	5.44	46.0
2o	51.85	6.13	0.38	−1.6	100	3.8	98.76	5.04	17.1
2p	51.85	7.79	0.24	−2.6	100	4.7	99.08	4.87	12.6
1Aa	50.16	5.31	−0.02	−1.1	100	2.9	99.62	6.68	14.2
1Ab	50.16	5.35	0.00	−1.1	100	2.9	99.40	6.33	49.2
1B	50.16	5.73	−0.01	−1.2	100	3.1	99.57	6.82	10.7
1C	50.16	5.94	0.46	−1.2	100	3.9	98.76	5.76	36.4
NESS06SM	59.39	5.25	0.50	−1.2	100	3.0	98.39	5.68	46.1
SM-11	56.15	6.09	0.27	−1.3	100	3.7	99.00	5.11	37.6
AM6538	105.21	5.94	−0.29	−1.5	100	3.8	99.73	5.98	23.4
Rimonabant	50.16	5.45	0.07	−1.2	100	2.9	99.28	6.45	48.7

[a]TPSA represents the polar surface area (Å^2) of the molecule.

[b]Extent of brain penetration based on ratio of total drug concentrations in tissue and plasma at steady-state conditions.

[c]Rate of passive diffusion-permeability PS represents permeability-surface area product and is derived from the kinetic equation of capillary transport.

[d]HIA represents the human intestinal absorption, expressed as percentage of the molecule able to pass through the intestinal membrane.

[e]Prediction of volume of distribution (Vd) of the compound in the body.

1Ab, **1B** and **1C** (TPSA = 50.16 Å^2; cLogP = 5.31–5.94) and with rimonabant (TPSA = 50.16 Å^2; cLogP = 5.45). On the other hand, **2a**, **2e**, **2i** and **2m** were endowed with a more drug-like lipophilicity over AM6538 (TPSA = 105.21 Å^2; cLogP = 5.94) but featuring lower TPSA values. In addition, these piperidine derivatives were characterized by the better pharmacokinetic profile with respect to the other congeners, exhibiting also increased oral bioavailability (%F = 49.2–90.0) with respect to the previous prototypes (%F = 10.7–49.2). Moreover, the piperidine-containing molecules experienced an improved bioavailability also in comparison with the references AM6538 and rimonabant (%F = 23.4–48.7). On the other hand, **2a**, **2e**, **2i** and **2m**, as well as most of the other analogues and the related prototypes, proved to pass the blood–brain barrier displaying adequate logBB and logPS values (recommended ranges as follows: $0 < \text{LogBB} < 1.5$; $-3 < \text{LogPS} < -1$). According to our calculations, only AM6538 was predictive inactive in terms of BBB permeation ability. Notably, only some compounds exhibited unfavoured BBB permeation probably because of the too high cLogP, deeply over 5 (Lipinski rules). In particular, a number of derivatives bearing cyclohexyl or myrtanyl moieties (**2d**, **2h**, **2k**, **2l**, **2p**) were predicted to be accompanied by elevated lipophilicity (cLogP = 6.45–7.79) and therefore are predicted to be anchored at the cellular membranes, so as to highly bind to plasmatic proteins. As consequence, **2d**, **2h**, **2k**, **2l**, **2p** displayed low bioavailability (%F = 4.4–13.4). All the newly synthesized derivatives are able to be fully adsorbed at the human intestinal membrane (HIA).

Based on all these data together with those coming from molecular docking studies, the bioisosteric replacement benzene/pyrrole arranged by **2a–p** with respect to **1A–C** appears to be a proper choice when accompanied by an adequate Q substituent, such as the piperidine one, in order to improve the pharmacokinetic profile. On the contrary, more hydrophobic moieties, such as cycloalkyl groups, could lead to unfavoured lipophilicity values. Thus, pharmacodynamics properties of any further new analogues need to be carefully optimized accordingly, by a proper selection of a branched and polar moiety to be inserted in Q, in order to achieve a good hydrophilicity–lipophilicity balance.

4 | CONCLUSION

In the present work, we synthesized the three series of tricyclic pyrrolopyrazole compounds that differ mainly in the number of atoms bridging the pyrrole nitrogen to pyrazole ring that probably engenders conformational changes in these novel tricyclic scaffolds as those reported for prototypes **1Aa**, **1Ab**, **1B** and **1C**. SAR studies were conducted on the three series of newly synthesized compounds, namely **2a–h**, **2i–l** and **2m–p**. Any of the new compounds showed high affinity for CB_2 receptor with K_i values superior to 314 nM, whereas some of them showed moderate affinity for CB_1 receptor with K_i values inferior to 400 nM. Compound **2j** exhibited good affinity for CB_1 receptor ($K_i CB_1$ = 81 nM) and the highest CB_2/CB_1 selectively ratio (>12).

Docking studies carried out on such compounds were performed using the hCB_1 X-ray in complex with the close pyrazole analogue AM6538 and disclosed specific pattern of interactions related to the tricyclic pyrrolopyrazole scaffolds as CB_1 ligands. Our preliminary results point out the versatility of the 1,4-dihydropyrazolo[3,4-*a*]pyrrolizine-, 4,5-dihydro-1*H*-pyrazolo[4,3-*g*]indolizine- and 1,4,5,6-tetra hydropyrazolo[3,4-*c*]pyrrolo[1,2-*a*]azepine architectures to provide novel compounds for CB_1 interaction. The results reported in the present work pave the way for a further design process towards more potent and selective CB_1 ligands.

CONFLICT OF INTEREST

None of the authors have conflict of interest to declare.

ENDNOTES

[1] MOE: Chemical Computing Group Inc. Montreal. H3A 2R7 Canada. http://www.chemcomp.com.

[2] www.biosolveit.com.

REFERENCES

[1] P. H. Reggio, *Curr. Med. Chem.* **2010**, *17*, 1468.

[2] V. Di Marzo, M. Bifulco, L. De Petrocellis, *Nat. Rev. Drug Discov.* **2004**, *3*, 771.

[3] S. T. Boyd, *Pharmacotherapy* **2006**, *26*, 218S.

[4] P. Pacher, S. Batkai, G. Kunos, *Pharmacol. Rev.* **2006**, *58*, 389.

[5] J.-P. Gong, E. S. Onaivi, H. Ishiguro, Q.-R. Liu, P. A. Tagliaferro, A. Brusco, G. R. Uhl, *Brain Res.* **2006**, *1071*, 10.

[6] Y. Gaoni, R. Mechoulam, *J. Am. Chem. Soc.* **1964**, *86*, 1646.

[7] a) S. Han, J. Thatte, D. J. Buzard, R. M. Jones, *J. Med. Chem.* **2013**, *56*, 8224; b) M. A. Tabrizi, P. G. Baraldi, P. A. Borea, K. Varani, *Chem. Rev.* **2016**, *116*, 519.

[8] a) G. Murineddu, B. Asproni, G. A. Pinna, *Rec. Pat. CNS Drug Discov.* **2012**, *7*, 4; b) G. Murineddu, F. Deligia, A. Dore, G. Pinna, B. Asproni, G. A. Pinna, *Rec. Pat. CNS Drug Discov.* **2013**, *8*, 42.

[9] I. Racz, X. Nadal, J. Alferink, J. E. Banos, J. Rehnelt, M. Martin, B. Pintado, A. Gutierrez-Adan, E. Sanguino, J. Manzanares, A. Zimmer, R. J. Maldonado, *Neurosciences* **2008**, *28*, 12125.

[10] R. G. Pertwee, A. C. Howlett, M. E. Abood, S. P. H. Alexander, V. Di Marzo, M. R. Elphick, P. J. Greasley, H. S. Hansen, G. Kunos, K. Mackie, R. Mechoulam, R. A. Ross, *Pharmacol. Rev.* **2010**, *62*, 588.

[11] a) M. Rinaldi-Carmona, F. Barth, M. Hkaulme, D. Shire, B. Calandra, C. Congy, S. Martinez, J. Maruani, G. Neliat, D. Caput, P. Ferrara, P. Soubrie, J. C. Breliere, G. Le Fur, *FEBS Lett.* **1994**, *350*, 240; b) F. Barth, M. Rinaldi-Carmona, *Curr. Med. Chem.* **1999**, *6*, 745.

[12] D. Jones, *Nat. Rev. Drug Discov.* **2008**, *7*, 961.
[13] M. K. Sharma, P. R. Murumkar, A. M. Kanhed, R. Giridhar, M. R. Yadav, *Eur. J. Med. Chem.* **2014**, *79*, 298.
[14] A. Fulp, K. Bortoff, Y. Zhang, R. Snyder, T. Fennell, J. A. Marusich, J. L. Wiley, H. Seltzman, R. Maitra, *J. Med. Chem.* **2013**, *56*, 8066.
[15] S. Röver, M. Andjelkovic, A. Beńardeau, E. Chaput, W. Guba, P. Hebeisen, S. Mohr, M. Nettekoven, U. Obst, W. F. Richter, C. Ullmer, P. Waldmeier, M. B. Wright, *J. Med. Chem.* **2013**, *56*, 9874.
[16] N. Mainolfi, J. Powers, J. Amin, D. Long, W. Lee, M. E. McLaughlin, B. Jaffee, C. Brain, J. Elliott, J. M. Sivak, *J. Med. Chem.* **2013**, *56*, 5464.
[17] J.-M. Mussinu, S. Ruiu, A. C. Mulè, A. Pau, M. A. M. Carai, G. Loriga, G. Murineddu, G. A. Pinna, *Bioorg. Med. Chem.* **2003**, *11*, 251.
[18] G. Murineddu, S. Ruiu, J.-M. Mussinu, G. Loriga, G. E. Grella, M. A. M. Carai, P. Lazzari, L. Pani, G. A. Pinna, *Bioorg. Med. Chem.* **2005**, *13*, 3309.
[19] P. Lazzari, R. Distinto, I. Manca, G. Baillie, G. Murineddu, M. Pira, M. Falzoi, M. Sani, P. Morales, R. Ross, M. Zanda, N. Jagerovic, G. A. Pinna, *Eur. J. Med. Chem.* **2016**, *121*, 194.
[20] L. Luongo, E. Palazzo, S. Tambaro, C. Giordano, L. Gatta, M. A. Scafuro, F. Rossi, P. Lazzari, L. Pani, V. de Novellis, M. Malcangio, S. Maione, *Neurobiol. Dis.* **2010**, *37*, 177.
[21] a) A. Mastinu, M. Pira, G. A. Pinna, C. Pisu, M. A. Casu, R. Reali, S. Marcello, G. Murineddu, P. Lazzari, *Pharmacol. Res.* **2013**, *74*, 94; b) G. R. Fois, L. Fattore, G. Murineddu, A. Salis, G. Pintore, B. Asproni, G. A. Pinna, M. Diana, *Pharmacol. Res.* **2016**, *113*, 108.
[22] a) P. Lazzari, A. Pau, S. Tambaro, B. Asproni, S. Ruiu, G. Pinna, A. Mastinu, M. M. Curzu, R. Reali, M. E. H. Bottazzi, G. A. Pinna, G. Murineddu, *Cent. Nerv. Syst. Agents Med. Chem.* **2012**, *12*, 254; b) G. Murineddu, B. Asproni, S. Ruiu, F. Deligia, M. Falzoi, A. Pau, B. F. Y. Thomas, Y. Zhang, G. A. Pinna, L. Pani, P. Lazzari, *Open Med. Chem. J.* **2012**, *6*, 1; c) G. Pinna, G. Loriga, P. Lazzari, S. Ruiu, M. Falzoi, S. Frau, A. Pau, G. Murineddu, B. Asproni, G. A. Pinna, *Eur. J. Med. Chem.* **2014**, *82*, 281; d) G. Pinna, M. M. Curzu, A. Dore, P. Lazzari, S. Ruiu, A. Pau, G. Murineddu, G. A. Pinna, *Eur. J. Med. Chem.* **2014**, *85*, 747; e) V. Deiana, M. Gómez-Cañas, M. R. Pazos, J. Fernández-Ruiz, B. Asproni, E. Cichero, P. Fossa, E. Muñoz, F. Deligia, G. Murineddu, M. García-Arencibia, G. A. Pinna, *Eur. J. Med. Chem.* **2016**, *112*, 66; f) A. Dore, B. Asproni, A. Scampuddu, S. Gessi, G. Murineddu, E. Cichero, P. Fossa, S. Merighi, S. Bencivenni, G. A. Pinna, *Bioorg. Med. Chem.* **2016**, *24*, 5291; g) G. Ragusa, M. Gómez-Cañas, P. Morales, C. Rodríguez-Cueto, M. R. Pazos, B. Asproni, E. Cichero, P. Fossa, G. A. Pinna, N. Jagerovic, J. Fernández-Ruiz, G. Murineddu, *Eur. J. Med. Chem.* **2017**, *127*, 398.
[23] G. Pinna, G. A. Pinna, G. Chelucci, S. Baldino, *Synthesis* **2012**, *44*, 2798.
[24] a) R. A. Ross, H. C. Brockie, L. A. Stevenson, V. L. Murphy, F. Templeton, A. Makriyannis, R. G. Pertwee, *Br. J. Pharmacol.* **1999**, *126*, 665; b) A. Thomas, L. A. Stevenson, K. N. Wease, M. R. Price, G. Ballie, R. A. Ross, R. G. Pertwee, *Br. J. Pharmacol.* **2005**, *146*, 917.
[25] P. Lazzari, G. Loriga, I. Manca, G. A. Pinna, L. Pani, U.S. Patent Application US 2010/0215741, August 26, **2010**.
[26] T. Hua, K. Vemuri, M. Pu, L. Qu, G. W. Han, Y. Wu, S. Zhao, W. Shui, S. Li, A. Korde, R. B. Laprairie, E. L. Stahl, J.-H. Ho, N. Zvonok, H. Zhou, I. Kufareva, B. Wu, Q. Zhao, M. A. Hanson, L. M. Bohn, A. Makriyannis, R. C. Stevens, Z.-J. Liu, *Cell* **2016**, *167*, 750.
[27] a) H.-J. Böhm, *J. Comput. Aided Mol. Des.* **1992**, *6*, 61; b) H.-J. Böhm, *J. Comput. Aided Mol. Des.* **1994**, *8*, 243; c) M. Rarey, B. Kramer, T. Lengauer, G. Klebe, *J. Mol. Biol.* **1996**, *261*, 470.
[28] L. Bichmann, Y.-T. Wang, W. B. Fischer, *Comput. Biol. Chem.* **2014**, *53*, 308.
[29] a) I. Reulecke, G. Lange, J. Albrecht, R. Klein, M. Rarey, *Chem. Med. Chem.* **2008**, *3*, 885; b) N. Schneider, S. Hindle, G. Lange, R. Klein, J. Albrecht, H. Briem, K. Beyer, H. Claußen, M. Gastreich, C. Lemmen, M. Rarey, *J. Comput. Aided Mol. Des.* **2012**, *26*, 701.
[30] P. Fossa, E. Cichero, *Bioorg. Med. Chem.* **2015**, *23*, 3215.
[31] P. Ertl, B. Rohde, P. Selzer, *J. Med. Chem.* **2000**, *43*, 3714.
[32] Y. Cheng, W. H. Prusoff, *Biochem. Pharmacol.* **1973**, *22*, 3099.
[33] a) T. Tuccinardi, P. L. Ferrarini, C. Manera, G. Ortore, G. Saccomanni, A. Martinelli, *J. Med. Chem.* **2006**, *49*, 984; b) G. Menozzi, P. Fossa, E. Cichero, A. Spallarossa, A. Ranise, L. Mosti, *Eur. J. Med. Chem.* **2008**, *43*, 2627.
[34] E. Cichero, G. Menozzi, A. Spallarossa, L. Mosti, P. Fossa, *J. Mol. Model.* **2008**, *14*, 1131.
[35] Z. Shao, J. Yin, K. Chapman, M. Grzemska, L. Clark, J. Wang, D. M. Rosenbaum, *Nature* **2016**, *540*, 602.

SUPPORTING INFORMATION

Additional Supporting Information may be found online in the supporting information tab for this article.

How to cite this article: Asproni B, Manca I, Pinna G, et al. Novel pyrrolocycloalkylpyrazole analogues as CB_1 ligands. *Chem Biol Drug Des*. 2017;00:1–13. https://doi.org/10.1111/cbdd.13069